Electronic Supplementary Material (ESI) for Chemical Communications.

Supporting information

FeCoP nanosheets on NiO nanoparticles electrocatalysts: tuning and stabilizing active sites for water splitting

*Sundaramoorthy Marimuthu, Ayyavu Shankar and Govindhan Maduraiveeran**

Materials Electrochemistry Laboratory, Department of Chemistry, SRM Institute of Science and Technology, Kattankulathur, Tamil Nadu-603 203, India

*Corresponding Author E-mail: *maduraig@srmist.edu.in*

EXPERIMENTAL SECTION

Chemicals

Ferric chloride anhydrous ($FeCl_3$), cobalt (II) nitrate hexahydrate (Co $(NO_3).6H_2O$) and KOH pellets were purchased by Sigma-Aldrich. Nitric acid and sodium dihydrogen phosphate were obtained from Alfa-Aesar. All analytical grade chemicals were used exactly as they were obtained. All of the solutions in this investigation were made with pure water (18.2 M cm) taken from a NANO pure Diamond UV deionized water purification system.

Fabrication of 3D Iron-Cobalt Phosphides Nanosheets on Nickel Oxide Nanoparticles

To begin with, nickel electrode substrate (geometrical surface area: ~0.8 cm^2; dimension of 0.25 mm radius and 5.0 mm height) was washed with dilute HCl, ethanol, and deionized water to remove surface oxide and contaminants, and then dried in the air for subsequent use. First, NiO nanoparticles were grown on the Ni electrode (NiO NPs|Ni) by chemically pre-treated with 0.1 M nitric acid for 1.0 h.[1,2] Second, three-dimensional iron-cobalt phosphide nanosheets were electrochemically deposited[3] on nickel oxide nanoparticles by continuous applied potential (E_{app}) of 0.1 V vs Ag/AgCl for 40 min using a precursor mixture containing 0.075 M $FeCl_3$ + 0.025 M $Co(NO_3)_2.6H_2O$ + 0.075 M sodium dihydrogen phosphate + 0.1 M HNO_3. The overall metal concentration (Fe and Co) of 0.1 M with the suitable Fe/Co molar ratios (1:0, 3:1 (A), 1:1 (B), 1:3 (C), 0:1) in 0.1 M HNO_3. The developed FeCoP@NiO-based nanomaterials are denoted as 3D-$Fe_{1-x}Co_xP$-A NS@NiO NPs|Ni, 3D-$Fe_{1-x}Co_xP$-B NS@NiO NPs|Ni and 3D-$Fe_{1-x}Co_xP$-C NS@NiO NPs|Ni, where x= 0.25 (A), 0.50 (B) and 0.75 (C), respectively, based on the experimental solution. The electrodes were then washed with deionized water and dried in the air.

Characterization

Primarily, high resolution scanning electron microscope (HR-SEM) (Thermosceintific Apreo S) equipped with EDS (FEI QUANTA 200 with an accelerating voltage of 20 kV) was utilized for studying surface morphology of the nanostructures. Transmission electron microscopic (TEM) and high-resolution transmission electron microscopic (HRTEM) studies were conducted with a JEOL 2010F TEM. X-ray diffraction (XRD) analysis were performed by using a PANanalyticalXpert Pro diffractometer with a Ni filtered monochromatic Cu Kr (1.5406 Å, 2.2 KW Max). X-ray photoelectron spectroscopic (XPS) studies were employed with a-PHI Versaprobe III to understand the chemical state and composition of the catalysts.

All electrochemical experiments were conducted using standard three electrode cells, with Ag/AgCl (3.0 KCl) employed as the reference electrode, the platinum coil served as the counter electrode, and the nickel substrate acted as the working electrode. The EIS test was used to investigate the kinetics of the OER process in the frequency range of 100 kHz - 50 MHz. The electrochemical impedance data was fitted using EC lab software. The following equation was used to convert all voltages to ($E_{(RHE)} = E_{(Ag/AgCl)} + 0.059\ pH + E^0$, where $E^0 = 0.197$ V at 25 °C). The mass loading m (g cm^2) of the catalysts and the measured current density j (A cm^2) at different overpotential (mass activity = j/m) were used to calculate the mass activity value (A g^{-1}).

The electrochemical active surface area (ECSA) of the as-developed electrodes was calculated using double-layer capacitance (C_{dl}) and specific capacitance (C_S) is 0.04 mF cm^{-2}, both of which were measured using cyclic voltammetry (CV) at different scan rates, starting from 10 to 125 mV s^{-1}.

$$ECASA = C_{dl} / C_S \quad (1)$$

The Turn over frequency (TOF) was calculated using of Eqn. (2) and (3).

$$n = m_{mass} / M \quad (2)$$

$$TOF = JA / 4Fn \quad (3)$$

where "n" is the number of moles of the active sites, "m_{mass}" means catalyst loading and "M" represents molar mass of catalysts. "J" describes the current density at overpotential (η) of ~0.158 V in A cm^{-2}, "A" means surface area of the nickel substrate (~0.81 cm^2), "F" represents the Faraday constant (96485 C mol^{-1}), respectively.

Table S1. Comparison of the OER and HER performance of 3D-$Fe_{1-x}Co_xP$-A NS@NiO NPs on nickel with the recently reported catalysts.

S. No	Materials	Synthetic method	Overpotential (η) (mV) OER	Overpotential (η) (mV) HER	Current Density (mA cm^{-2})	Ref
1	CFeCoNiP/NF	Electrodeposition	250	37	10	S4
2	FeNi LDH/FeNi foil	Hydrothermal	130	-	10	S5
3	CoFe-P/NF	Electrodeposition	257	45	10	S6
4	CoO_x –CoSe/NF	Electrodeposition	300	90	10	S7
5	NiFeCoPi/P	Electrodeposition	299	98	10	S8
6	Co-Ni-P-2	Electrodeposition	340	103	10	S9
7	NiFe@Ni(Cu)/NF	Electrodeposition	209	36	10	S10
8	$Co_{0.9}Fe_{0.1}$-Se/NF	Electrodeposition	245	135	10	S11
9	NiSP/NF	Electrodeposition	259	93	10	S12
10	Ni-Fe-Co-S	Electrodeposition	207	106	10	S13
11	$Ni(OH)_2$/NF	Electrodeposition	166	187	20	S14
12	Fe_4Ni-Se/NF	Electrodeposition	207	93	10	S15
13	NiCoMnFe–P	Electrodeposition	279	300	10	S16
14	Ni-Cu/copper sheets	Electrodeposition	290	76	10	S17
15	3D-$Fe_{1-x}Co_xP$-A NS@NiO NPs|Ni	**Electrodeposition**	**158**	**74**	**10**	**This Study**

NF: nickel foam; LDH: layered double hydroxide; NPs: nanoparticles

Table S2. Comparison OER performance of the developed transition metal electrodes in this study is listed.

S. No	Electrodes	Onset potential / V (RHE)	OER η (mV) @ 10 mA cm^{-2}
1	3D-FeP NS@NiO NPs|Ni	1.33	173
2	3D-CoP NS@NiO NPs|Ni	1.37	179
3	NiP@NiO|Ni	1.44	289
4	CuP@NiO|Ni	1.58	426
5	FeS@NiO|Ni	1.37	176
6	FeSe@NiO|Ni	1.46	272
4	FeP |Cu	1.46	273
	FeP |SS	1.43	225
5	$Fe_{1-x}Co_xP$-A |Cu	1.58	400
6	$Fe_{1-x}Co_xP$-A |SS	1.57	381
7	IrO_2 |Ni	1.55	366
9	3D-$Fe_{1-x}Co_xP$-A NS@NiO NPs|Ni	1.35	158
10	3D-$Fe_{1-x}Co_xP$-B NS@NiO NPs|Ni	1.45	258
11	3D-$Fe_{1-x}Co_xP$-C NS@NiO NPs|Ni	1.40	215
SS:Stainless Steel; Cu-Copper; Ni- Nickel electrode; Fe/Co molar ratios ("**A**" =3:1 (x=0.25), "**B**" =1:1 (x=0.50), "**C**" =1:3 (x=0.75))			

Table S3. EIS data derived from Nyquist plots of **Fig. 2(e).**

Electrodes	E_{app} **/ V**	R_s **[Ω cm²]**	R_p **[Ω cm²]**	C **[mF cm²]**
3D-FeP NS@NiO NPs|Ni		3.91	5.95	2.67
3D-$Fe_{1-x}Co_xP$-A NS@NiO NPs|Ni		3.38	3.40	74.08
3D-$Fe_{1-x}Co_xP$-B NS@NiO NPs|Ni	1.63	3.44	6.83	9.68
3D-$Fe_{1-x}Co_xP$-C NS@NiO NPs|Ni		4.18	13.54	14.79
3D-CoP NS@NiO NPs|Ni		2.89	14.54	54.70

Table S4. EIS data derived from Nyquist plots of **Fig. 3(b).**

Electrodes	E_{app} / V	R_s [Ω cm^2]	R_p [Ω cm^2]	C [mF cm^2]
3D-$Fe_{1-x}Co_xP$-ANS@NiO NPs|Ni	-1.18	4.89	34.99	3.61
	-1.25	4.47	15.89	3.66
	-1.31	4.37	7.98	3.97

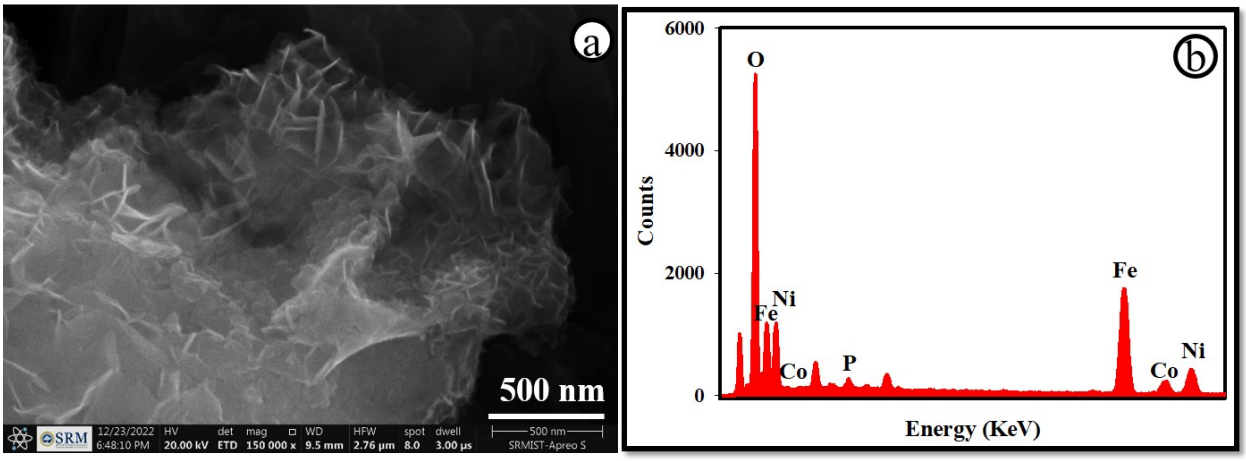

Fig. S1. HRSEM image (a), and EDX spectra (b) of the 3D-$Fe_{1-x}Co_xP$-A NS@NiO NPs|Ni electrode.

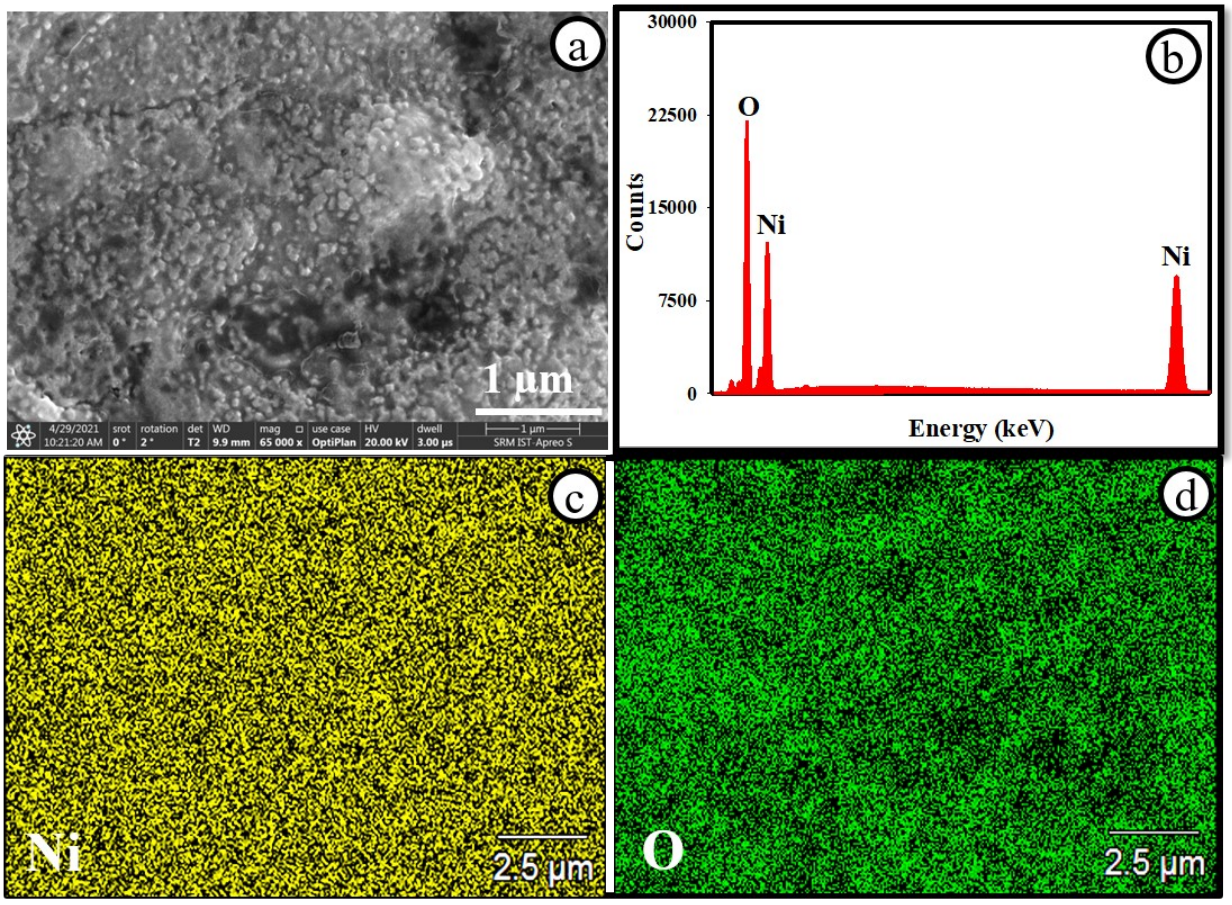

Fig. S2. SEM image (a), EDX spectrum (b), and elemental mapping of Ni (c) and O (d) for the NiO NPs|Ni electrode.

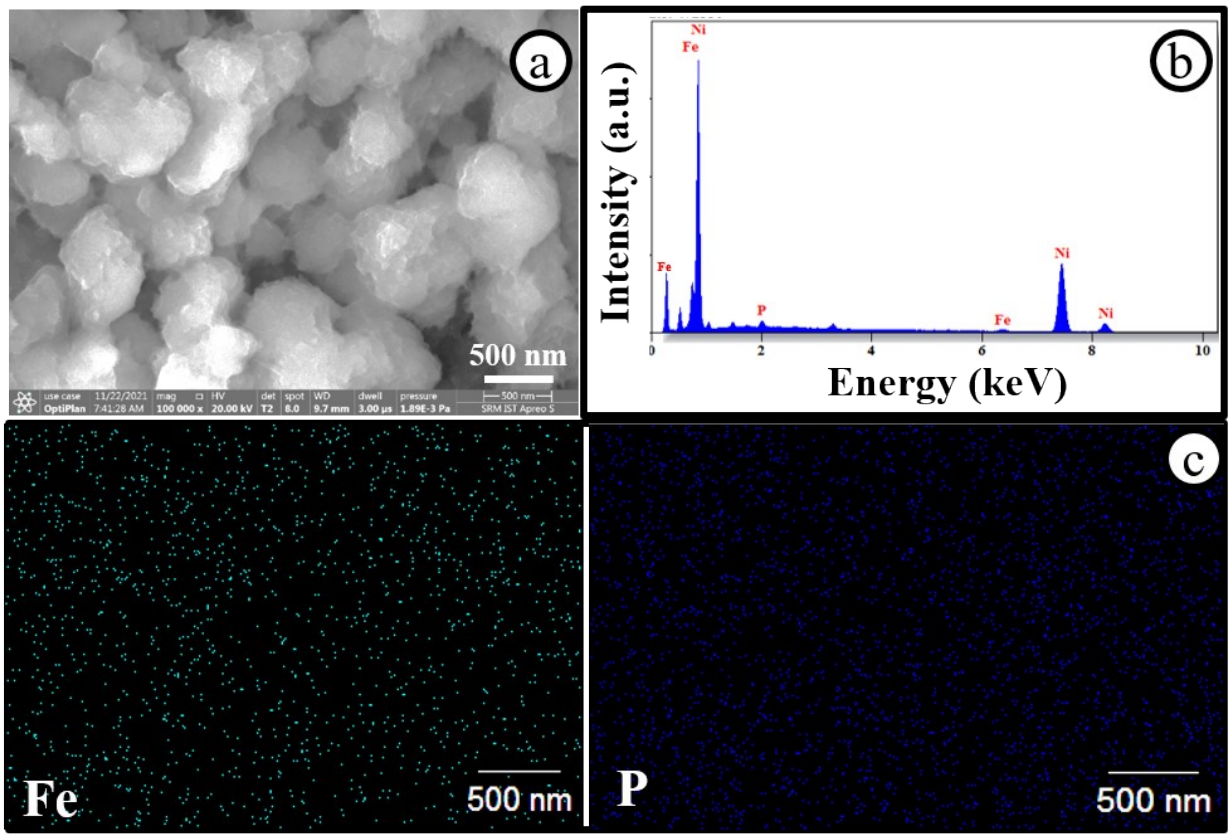

Fig. S3. SEM image (a), EDX spectra (b) and elemental mapping of Fe, and P (c) for the 3D-FeP NS@NiO NPs|Ni electrode.

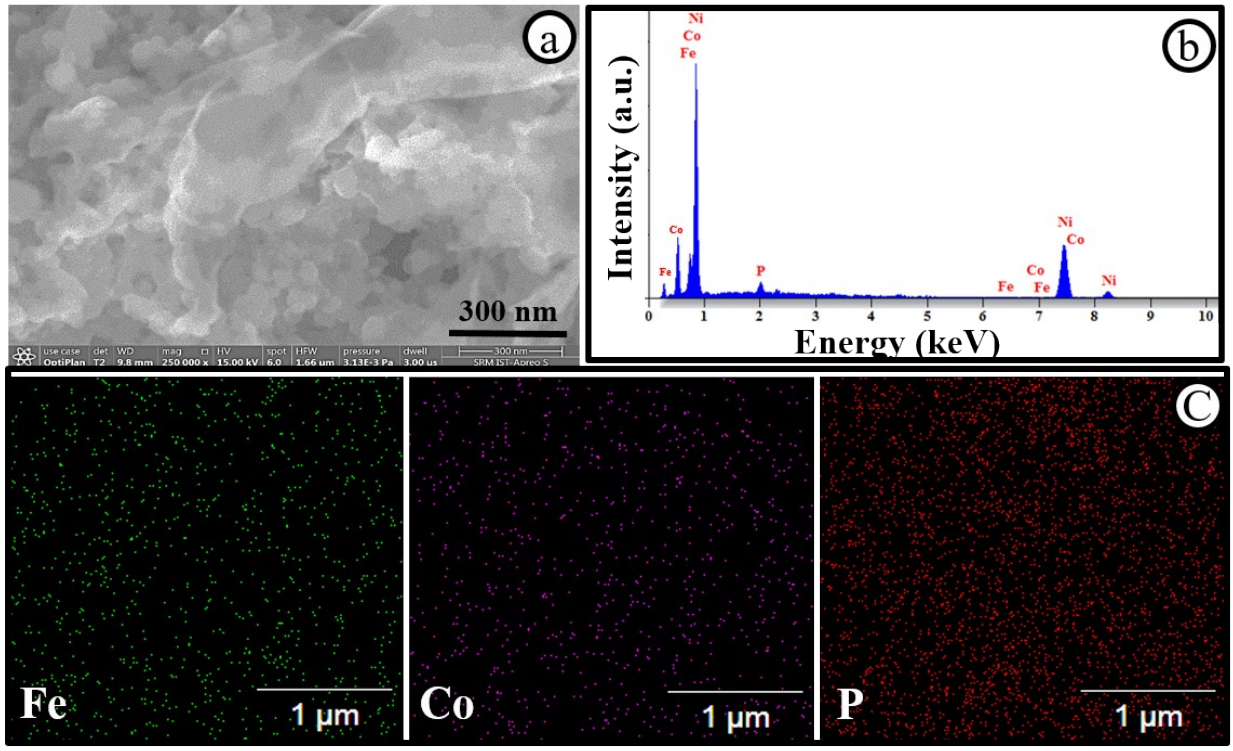

Fig. S4. SEM image (a), EDX spectra (b) and elemental mapping of Fe, Co and P (c) for the 3D-$Fe_{1-x}Co_xP$-B NS@NiO NPs|Ni electrode.

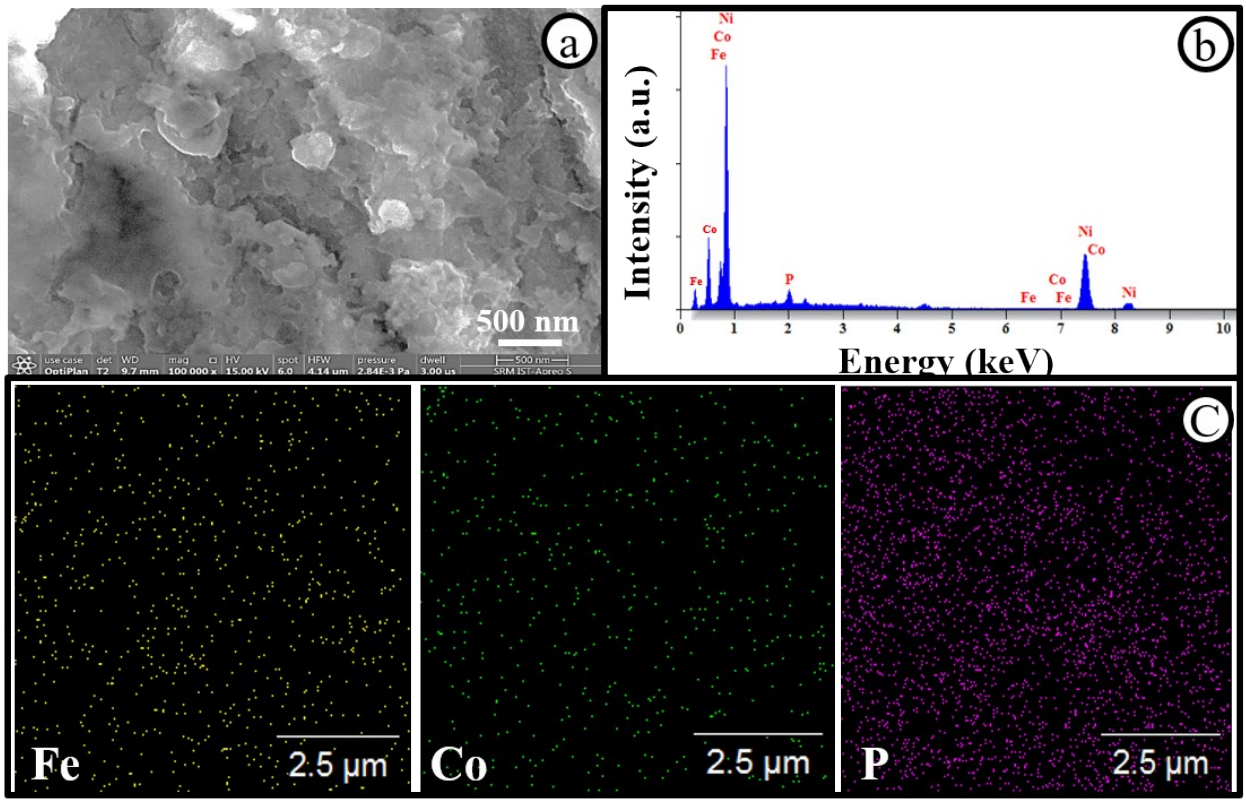

Fig. S5. SEM image (a), EDX spectra (b) and elemental mapping of Fe, Co and P (c) for the 3D-$Fe_{1-x}Co_xP$-C NS@NiO NPs|Ni electrode.

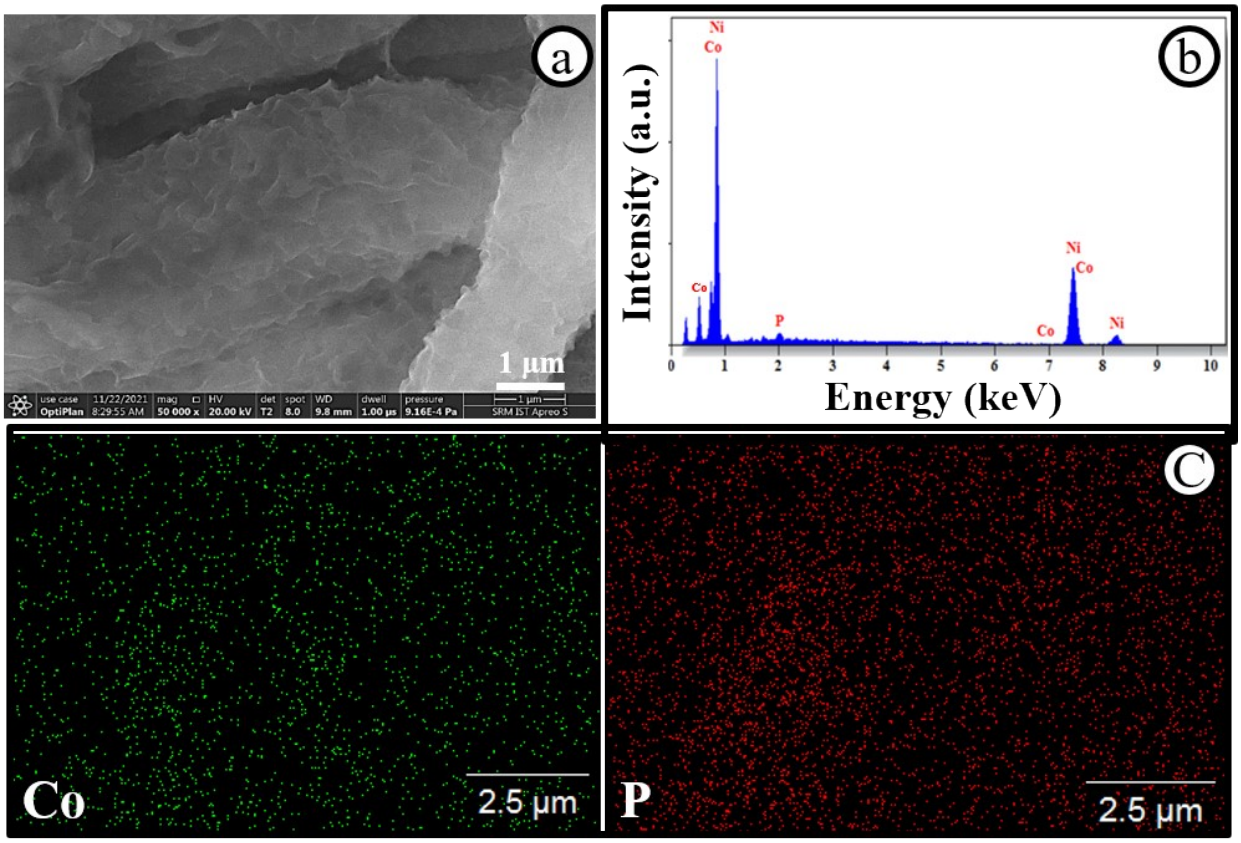

Fig. S6. SEM image (a), EDX spectra (b) and elemental mapping of Co, and P (c) for the 3D-CoP NS@NiO NPs|Ni electrode.

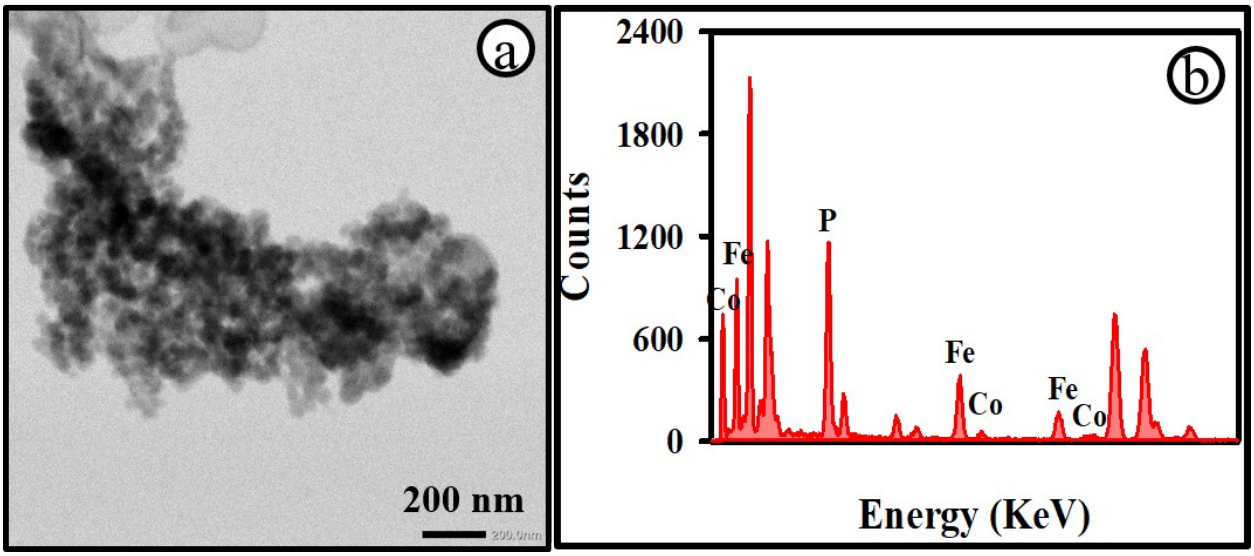

Fig. S7. TEM image (a) and EDX spectrum (b) of the 3D-$Fe_{1-x}Co_xP$-A NS@NiO NPs.

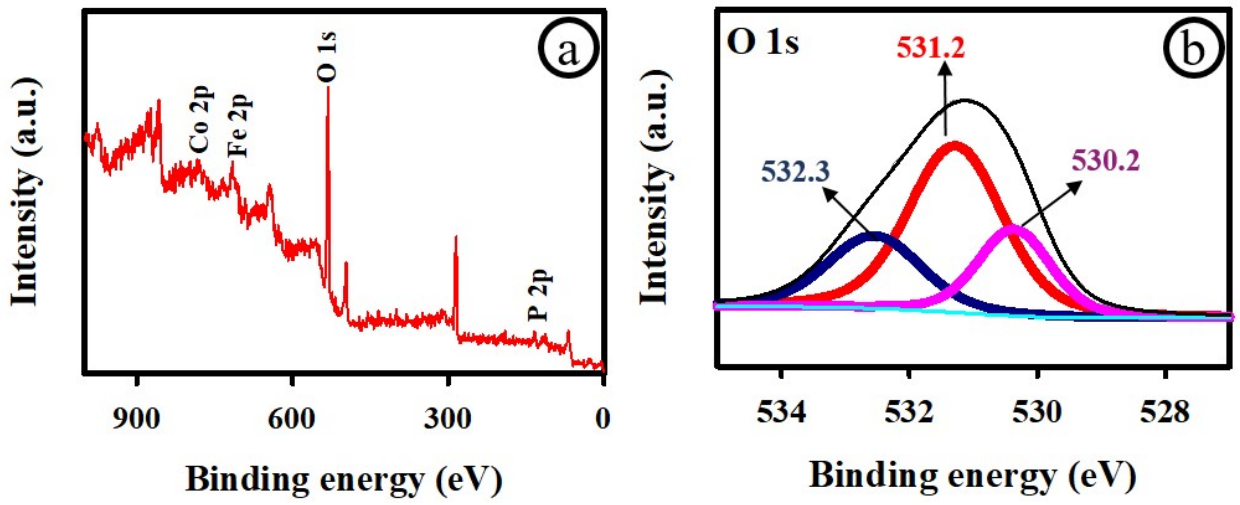

Fig. S8. XPS Survey spectra (a) and O 1s of the 3D-$Fe_{1-x}Co_xP$-A NS@NiO NPs|Ni electrode (b).

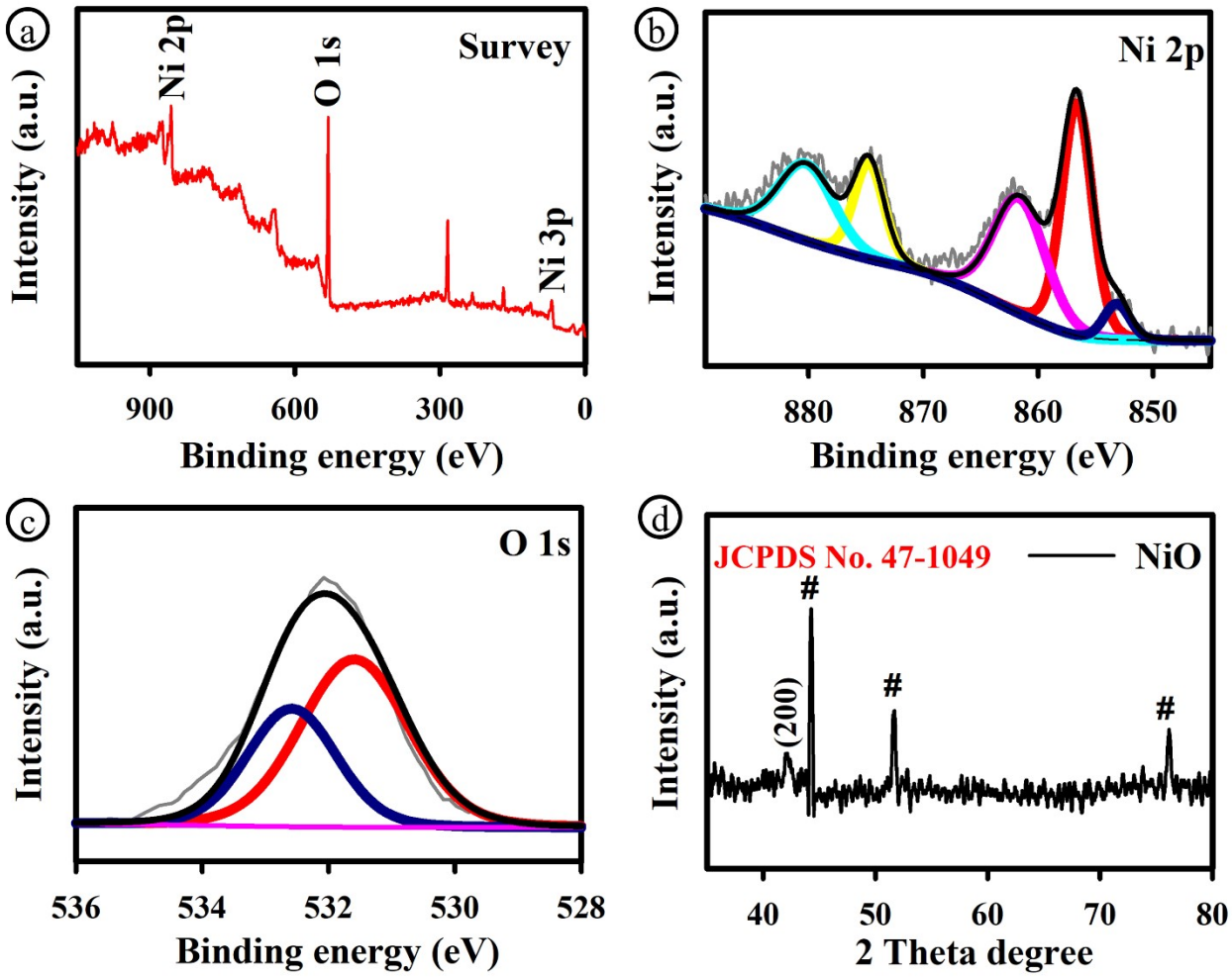

Fig. S9. XPS survey spectra (a), Ni 2p (b) and O 1s (c) for the NiO|Ni electrode. XRD spectrum of the NiO|Ni electrode (d), where #-marked peaks corresponded to Ni substrate.

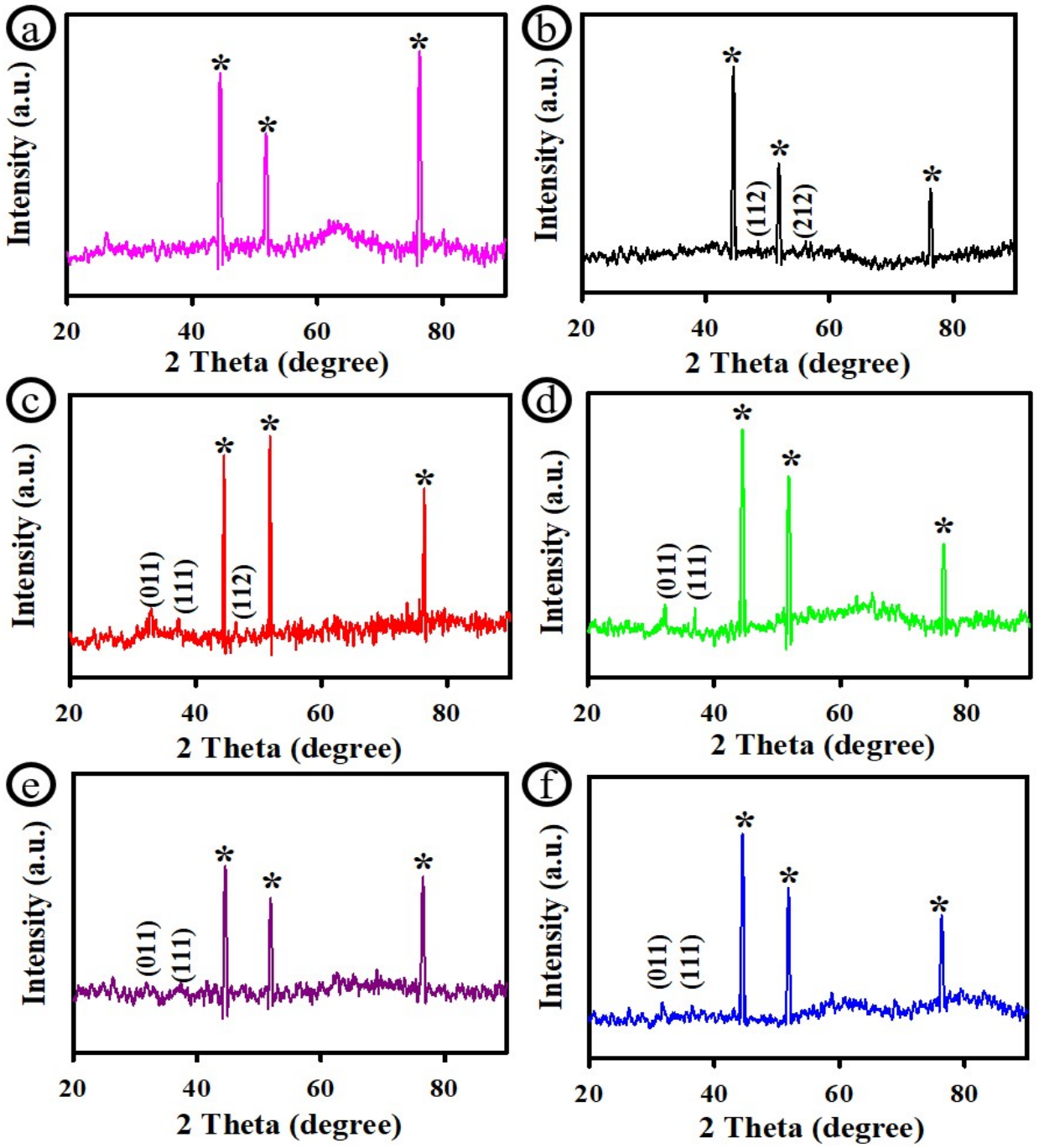

Fig. S10. XRD pattern of the bare Ni (a), 3D-FeP NS@NiO NPs|Ni (b), 3D-$Fe_{1-x}Co_xP$-A NS@NiO NPs|Ni (c), 3D-$Fe_{1-x}Co_xP$-B NS@NiO NPs|Ni (d), 3D-$Fe_{1-x}Co_xP$-C NS@NiO NPs|Ni (e), and 3D-CoP NS@NiO NPs|Ni (f) nanostructured electrodes.

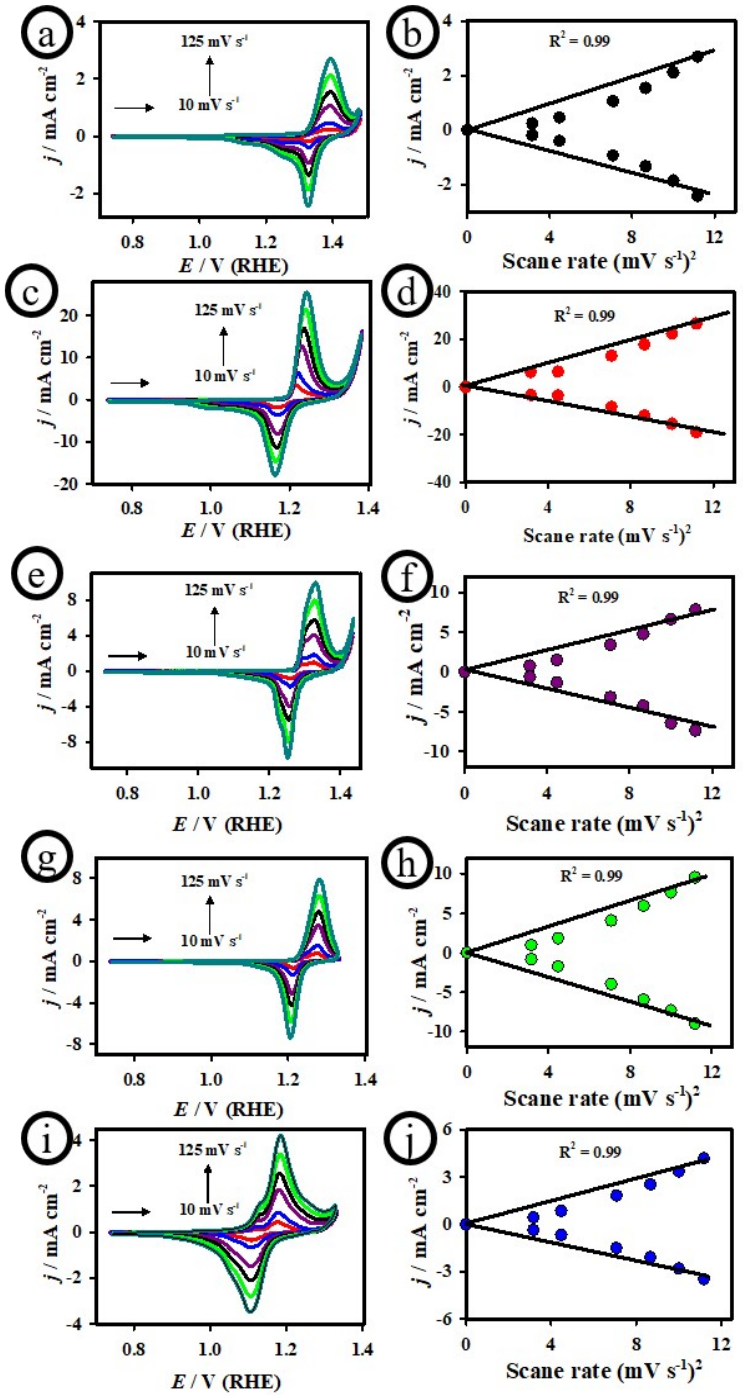

Fig. S11. CV curves 3D-FeP NS@NiO NPs|Ni (a), 3D-$Fe_{1-x}Co_xP$-A NS@NiO NPs|Ni (c), 3D-$Fe_{1-x}Co_xP$-B NS@NiO NPs|Ni (e), 3D-$Fe_{1-x}Co_xP$-C NS@NiO NPs|Ni (g), and 3D-CoP NS@NiO NPs|Ni (i) at different scan rates recorded in 1.0 M KOH starting from 10 to 125 mV s^{-1} and the corresponding plot of peak current density vs square root of the scan rate.

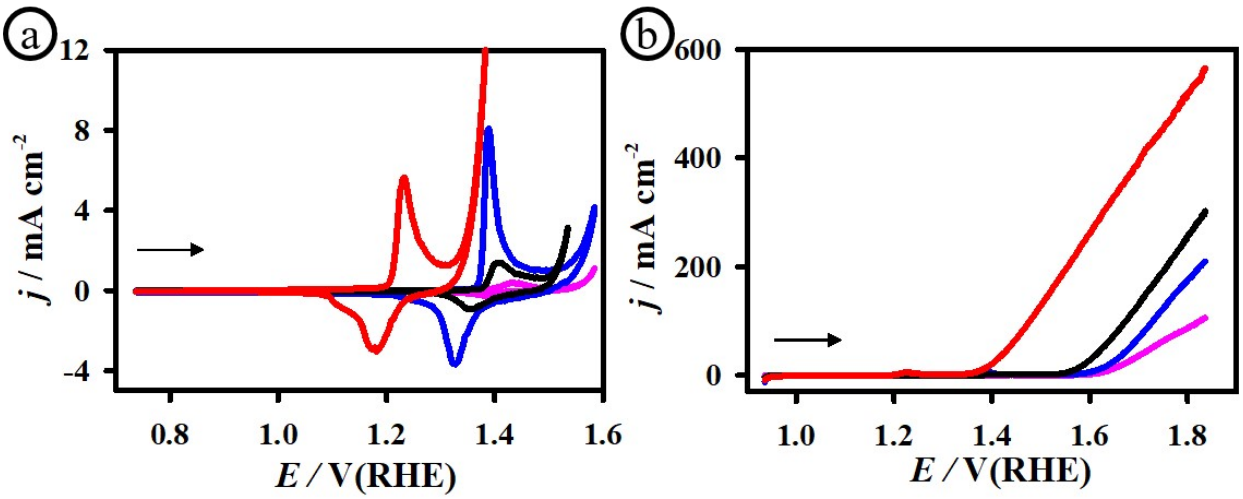

Fig. S12. CV (a) and LSV (b) curves of the bare Ni electrode (pink), NiO NPs|Ni (blue), FeCoP-A |Ni (black) and 3D-$Fe_{1-x}Co_xP$-A NS@NiO NPs|Ni (red) recorded in 1.0 KOH.

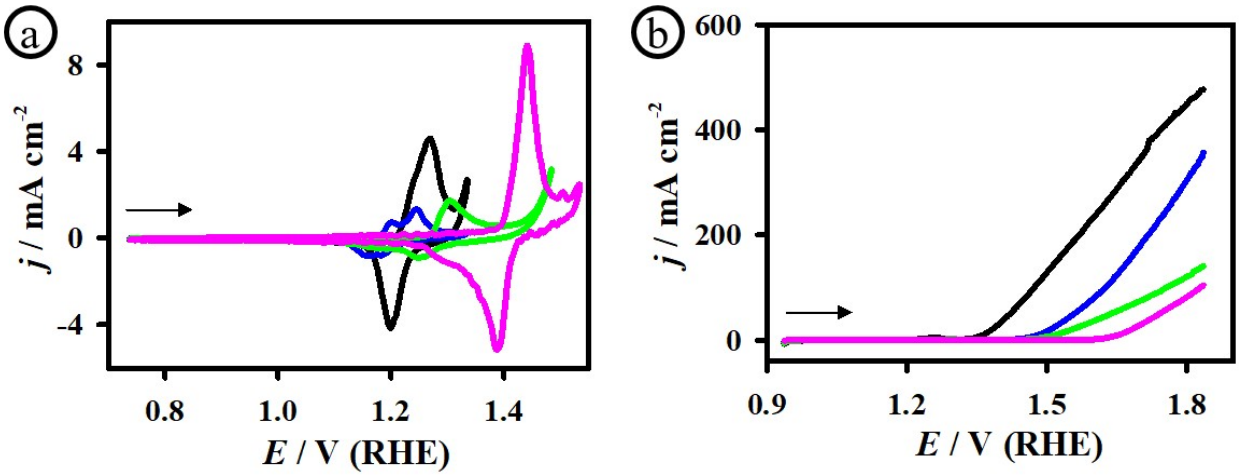

Fig. S13. CV curves (a) and LSV curves (b) of the 3D-FeP NS@NiO NPs|Ni (black), 3D-CoP NS@NiO NPs|Ni (blue), NiP@NiO|Ni (green) and CuP@NiO|Ni (pink) electrodes recorded in 1.0 M KOH electrolyte at a scan rate of 20 mV s^{-1}.

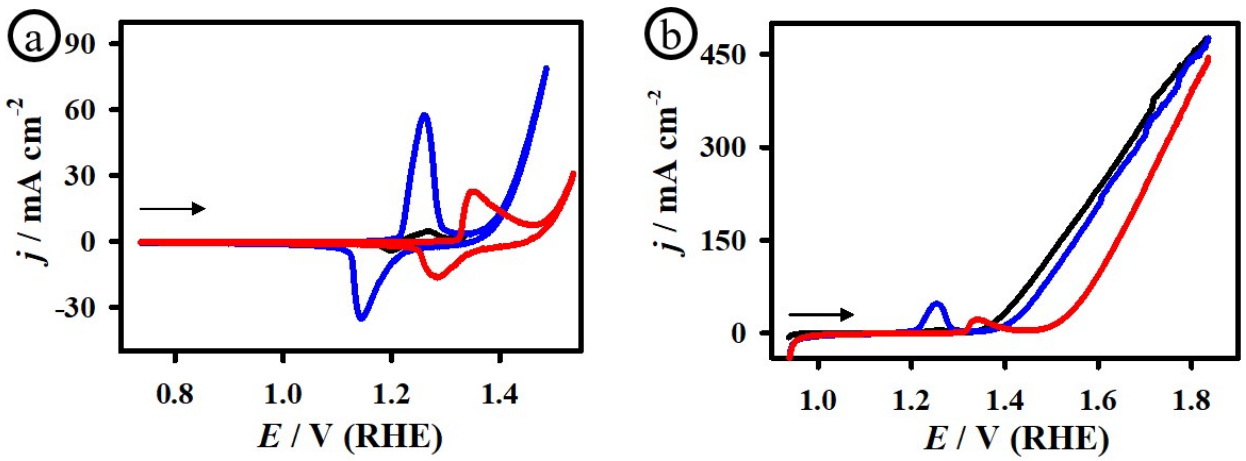

Fig. S14. CV curves (a), and LSV curves (b) of the 3D-FeP NS@NiO NPs|Ni (black), FeS@NiO|Ni (blue), and FeSe@NiO|Ni (red) electrodes recorded in 1.0 M KOH at a scan rate of 20 mV s^{-1}.

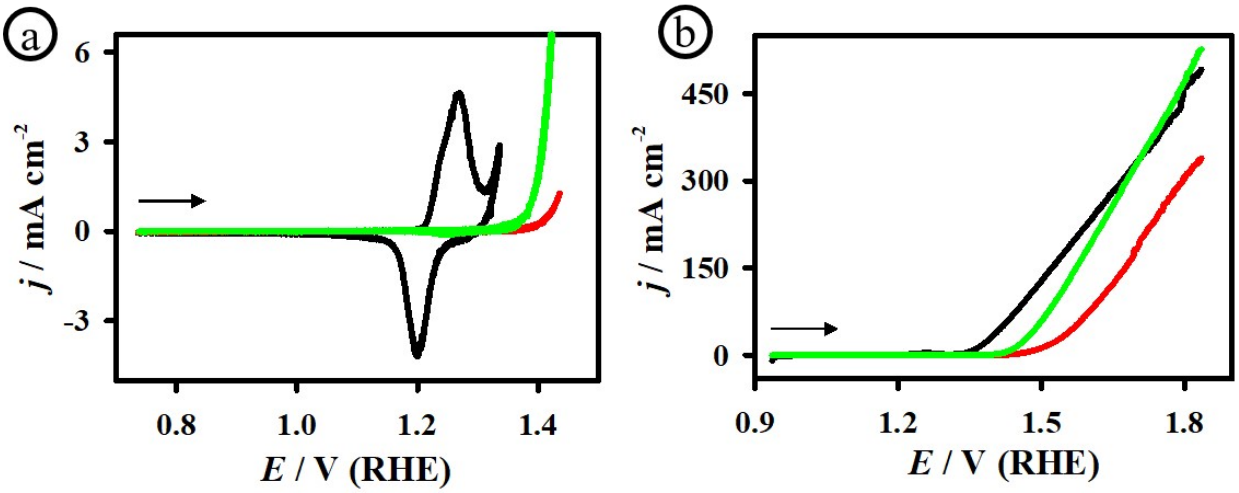

Fig. S15. CV curves (a), and LSV curves (b) of the 3D-FeP NS@NiO NPs|Ni (black), FeP|Cu (red), and FeP|SS (green) electrodes recorded in 1.0 M KOH at a scan rate of 20 mV s^{-1}.

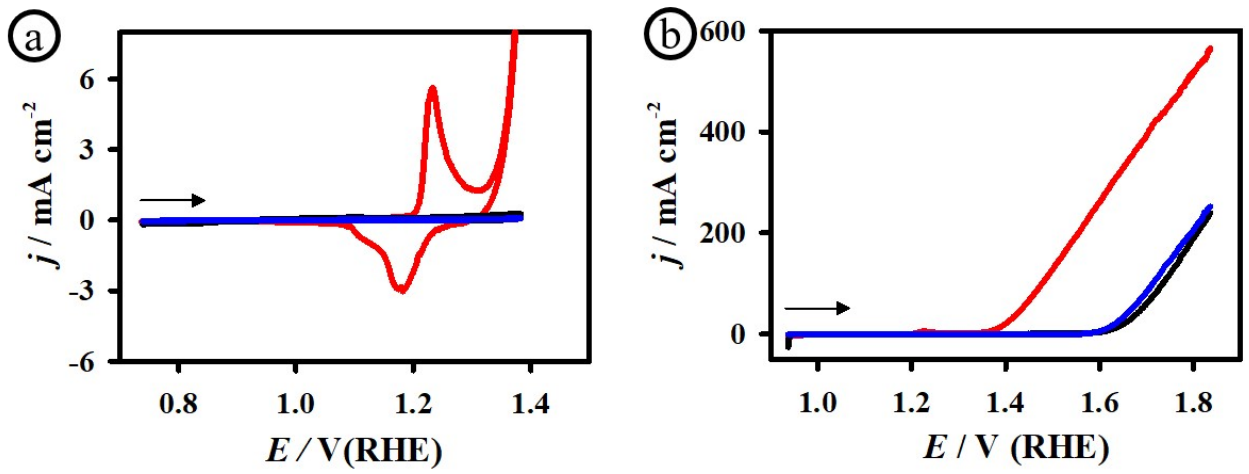

Fig. S16. CV curves (a), and LSV curves (b) of the 3D-$Fe_{1-x}Co_xP$-A NS@NiO NPs|Ni (red), FeCoP-A|Cu (black), and FeCoP-A|SS (blue) electrodes recorded in 1.0 M KOH at a scan rate of 20 mV s^{-1}.

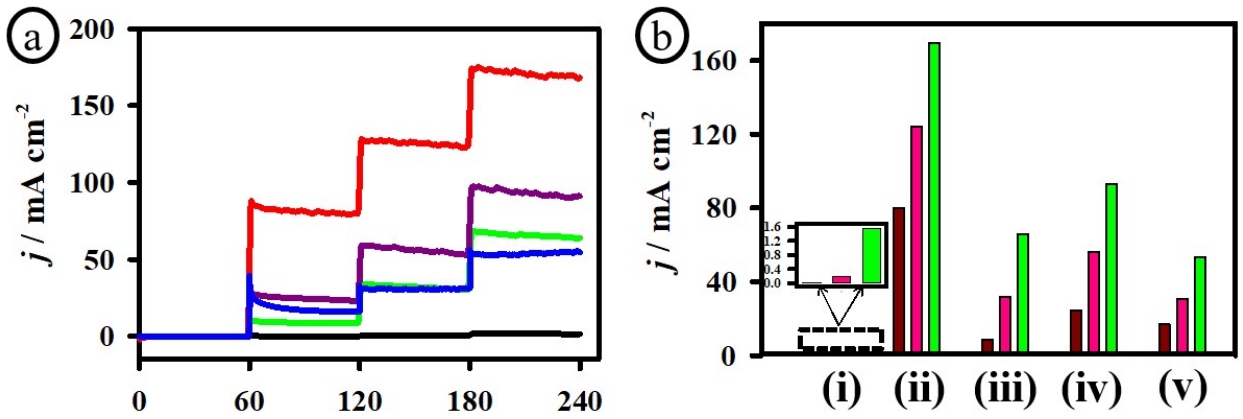

Fig. S17. (a) Chronoamperometric response and plot of current density vs various electrodes of 3D-FeP NS@NiO NPs|Ni (black, i), 3D-$Fe_{1-x}Co_xP$-A NS@NiO NPs|Ni (red, (ii)), 3D-$Fe_{1-x}Co_xP$-B NS@NiO NPs|Ni (green, (iii)), 3D-$Fe_{1-x}Co_xP$-C NS@NiO NPs|Ni (violet, (iv)) and 3D-CoP NS@NiO NPs|Ni (blue, (v)) on nickel electrodes at different applied potentials of 1.43 (dark red), 1.47 (dark pink), and 1.51 V (green) vs RHE.

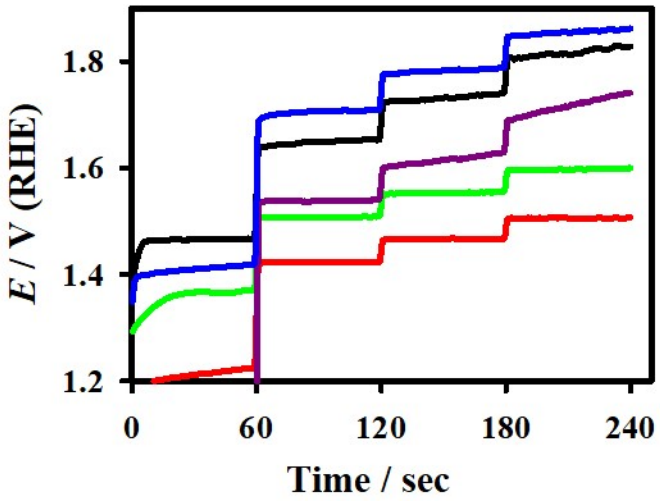

Fig. S18. (a) Chronopotentiometric response of the the 3D-FeP NS@NiO NPs|Ni (black), 3D-$Fe_{1-x}Co_xP$-A NS@NiO NPs|Ni (red), 3D-$Fe_{1-x}Co_xP$-B NS@NiO NPs|Ni (green), 3D-$Fe_{1-x}Co_xP$-C NS@NiO NPs|Ni (violet) and 3D-CoP NS@NiO NPs|Ni (blue) on nickel electrodes at different applied current densities of 50, 100, and 150 mA cm^{-2}.

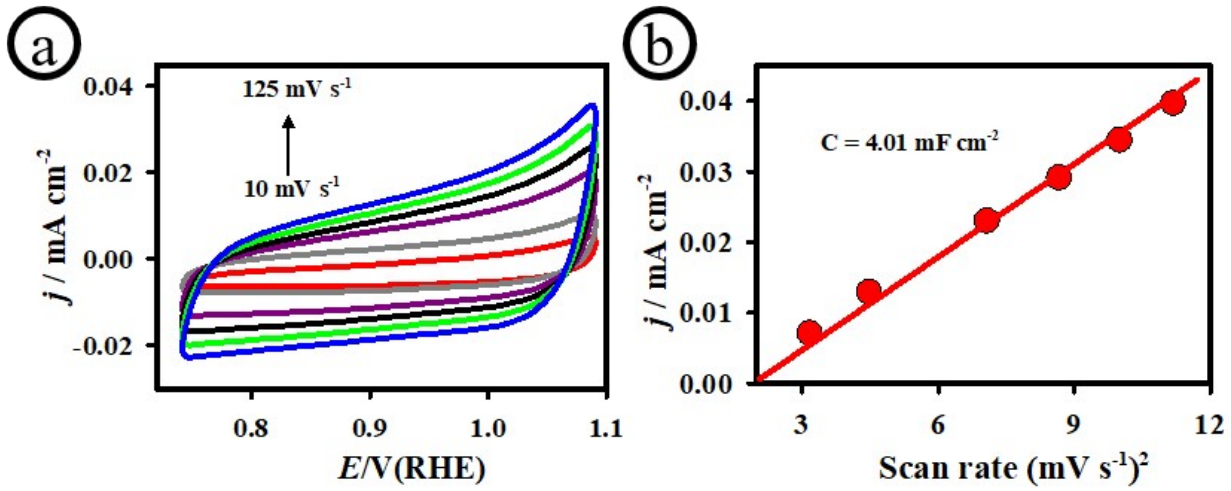

Fig. S19. (a) CV curves of the 3D-$Fe_{1-x}Co_xP$-A NS@NiO NPs|Ni electrode recorded in 1.0 M KOH solution at different scan rates from 10 to 125 mV s^{-1}. (b) The corresponding plot of anodic current density vs scan rates.

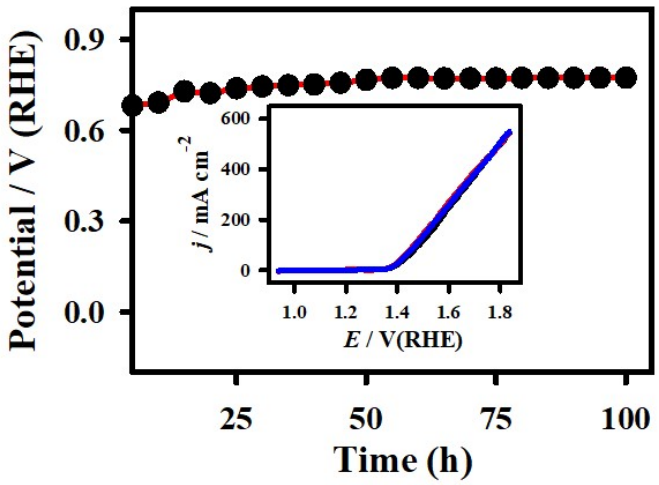

Fig. S20. Chronopotentiometric response of the 3D-$Fe_{1-x}Co_xP$-A NS@NiO NPs|Ni electrode at applied potential of 1.47 V for 100 h. Inset; LSV curves of the different brand-new 3D-$Fe_{1-x}Co_xP$-A NS@NiO NPs|Ni electrodes measured in 1.0 M KOH at a scan rate of 20 mV s^{-1}.

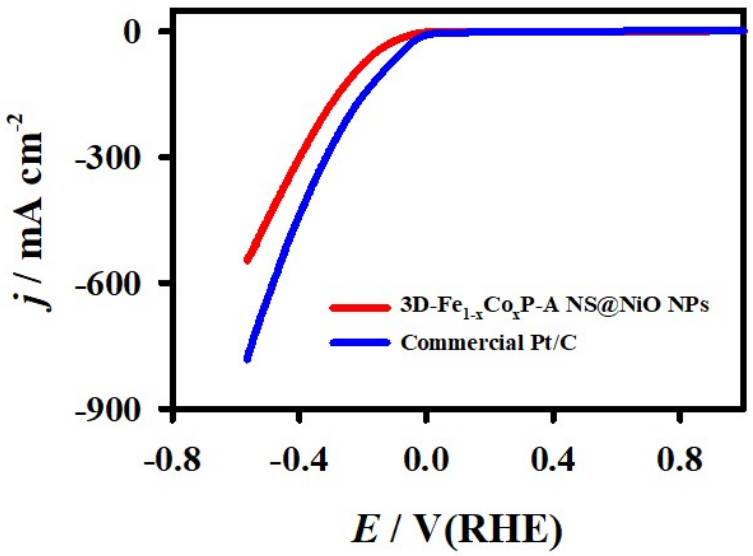

Fig. S21. HER polarization curves of 3D-$Fe_{1-x}Co_xP$-A NS@NiO NPs|Ni (red) and Pt/C (blue) electrodes recorded in 1.0 KOH.

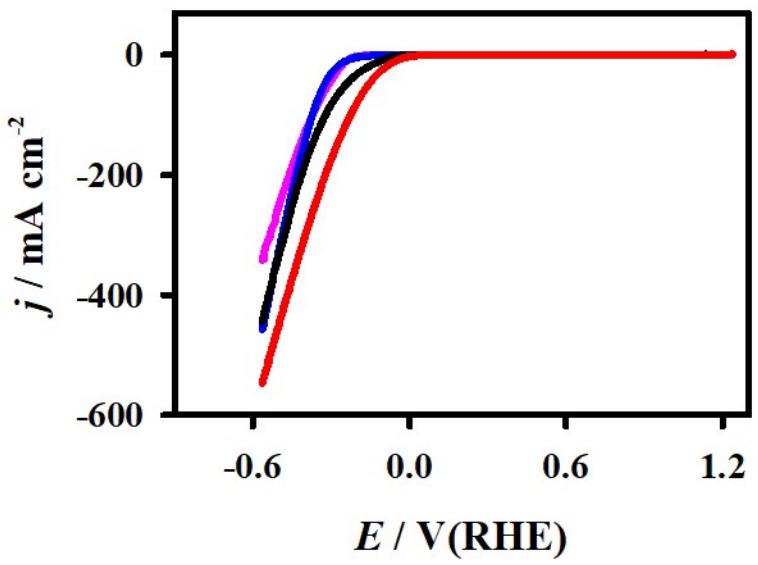

Fig. S22. LSV curve of the bare Ni electrode (pink), NiO NPs|Ni (blue), $Fe_{1-x}Co_xP$-A|Ni (black) and 3D-$Fe_{1-x}Co_xP$-A NS@NiO NPs|Ni (red) recorded in 1.0 KOH.

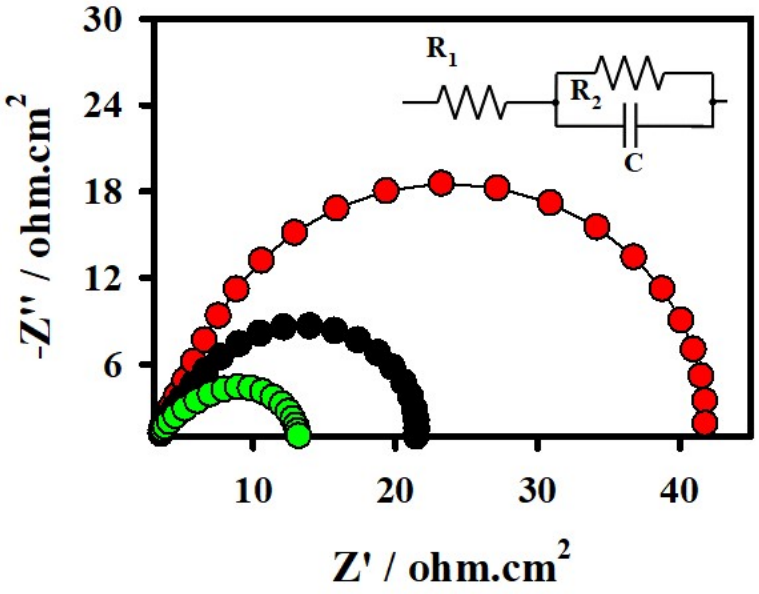

Fig. S23. Nyquist plots of 3D-$Fe_{1-x}Co_xP$-A NS@NiO NPs|Ni at different E_{apps} of -0.14 V (red), -0.21 V (black), and -0.27 V (green).

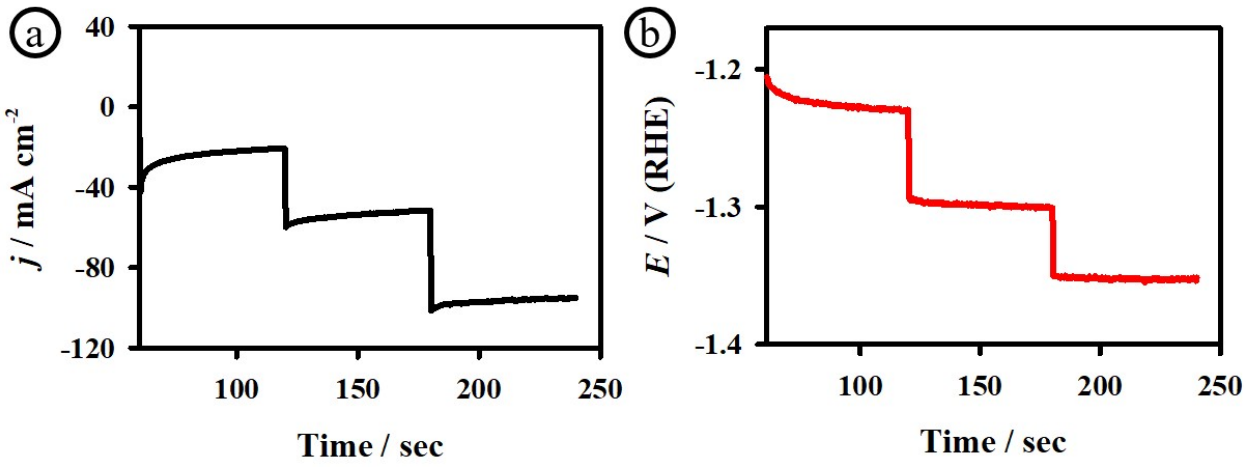

Fig. S24. (a) CA response of the 3D-$Fe_{1-x}Co_xP$-A NS@NiO NPs|Ni (black) electrode at different applied potentials of -1.18, -1.25 and -1.31 V vs. (RHE). (b) CP response of the 3D-$Fe_{1-x}Co_xP$-A NS@NiO NPs|Ni (red) electrode at different applied current densities of -50, -100, and -150 mA cm^{-2}.

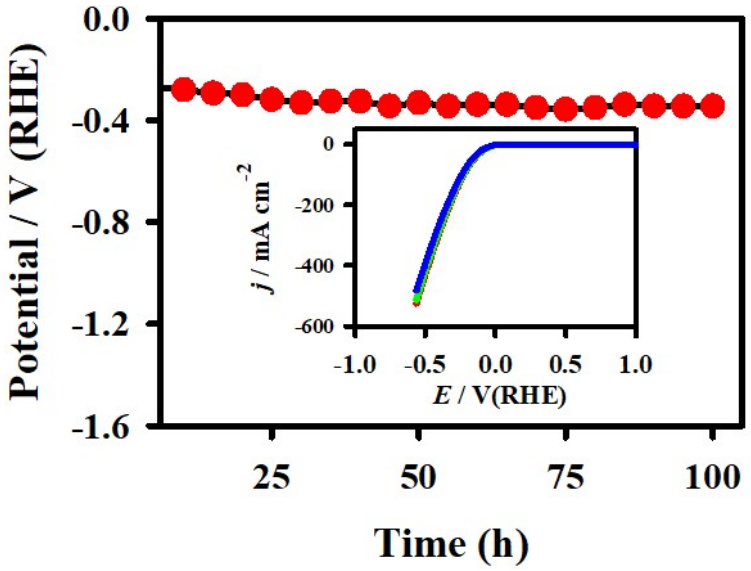

Fig. S25. CP curve of the 3D-$Fe_{1-x}Co_xP$-A NS@NiO NPs|Ni electrode recorded under j_{app} of ~10.0 mA cm^{-2}. Inset: Reproducible HER polarization curves of the three-brand new 3D-$Fe_{1-x}Co_xP$-A NS@NiO NPs|Ni electrodes.

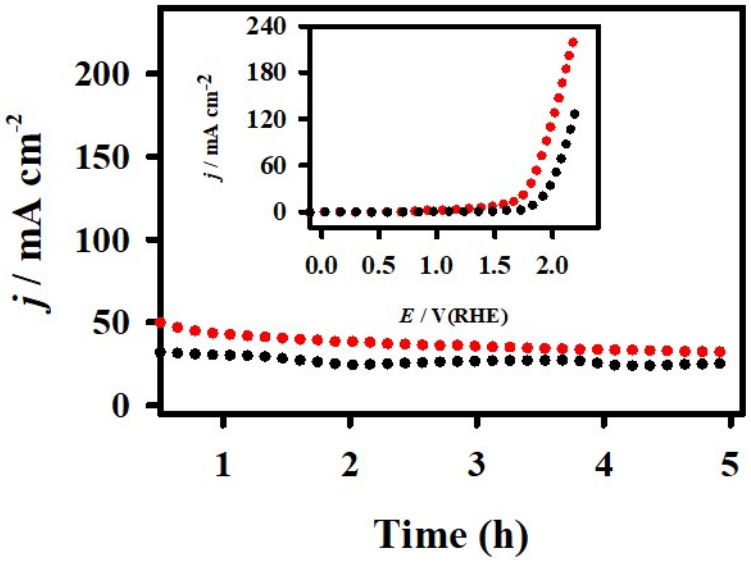

Fig. S26. CA curves of the 3D-$Fe_{1-x}Co_xP$-A NS@NiO NPs || 3D-$Fe_{1-x}Co_xP$-A NS@NiO NPs (red) and Pt/C || IrO_2 (black) electrodes for full water splitting. Inset; LSV curves of the 3D-$Fe_{1-x}Co_xP$-A NS@NiO NPs || 3D-$Fe_{1-x}Co_xP$-A NS@NiO NPs (red), and Pt/C || IrO_2 (black) electrodes. Electrolyte: 1.0 M KOH.

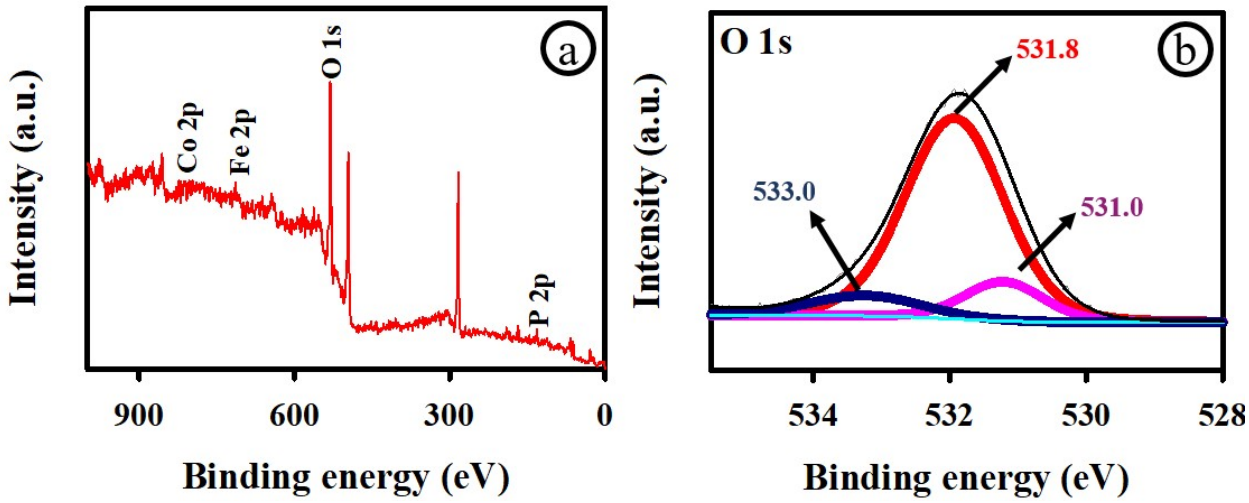

Fig. S27. XPS survey spectrum (a) and high-resolution O 1s XPS (b) spectra of 3D-$Fe_{1-x}Co_xP$-A NS@NiO NPs|Ni after had a long-term durability test.

References

S1 M. Arivazhagan and G. Maduraiveeran, *Materials Chemistry and Physics*, 2023, **295**, 127084.

S2 J. S. Dondapati, M. Govindhan and A. Chen, *Chemical Communications*, 2022, **58**, 11127–11130.

S3 Y. Shi, W.-M. Huang, J. Li, Y. Zhou, Z.-Q. Li, Y.-C. Yin and X.-H. Xia, *Nature Communications*, 2020, **11**, 4558.

S4 F.-T. Tsai, Y.-T. Deng, C.-W. Pao, J.-L. Chen, J.-F. Lee, K.-T. Lai and W.-F. Liaw, *Journal of Materials Chemistry A*, 2020, **8**, 9939–9950.

S5 Q. Xiang, F. Li, W. Chen, Y. Ma, Y. Wu, X. Gu, Y. Qin, P. Tao, C. Song, W. Shang, H. Zhu, T. Deng and J. Wu, *ACS Energy Letters*, 2018, **3**, 2357–2365.

S6 Donghong Duan, DeshengGuo, JieGao, ShibinLiu, YunfangWang, Journal of Colloid and Interface Science, 2022, 622, 250–260.

S7 X. Xu, P. Du, Z. Chen and M. Huang, Journal of Materials Chemistry A, 2016, **4**, 10933–10939.

S8 Y. Sun, C. Chang, S. Zhu, X. Liu, Y. Chen, Y. Tang, P. Wan and J. Pan, Industrial and Engineering Chemistry Research, 2021, **60**, 2070–2078.

S9 Y. Pei, Y. Yang, F. Zhang, P. Dong, R. Baines, Y. Ge, H. Chu, P. M. Ajayan, J. Shen and M. Ye, ACS Applied Materials and Interfaces, 2017, **9**, 31887–31896.

S10 Y. Li, K. Dastafkan, Q. Sun, Y. Ma, X. Wang, X. Yang, Z. Wang and C. Zhao, Electrochimica Acta, 2021, **379**, 138042.

S11 H. Ren, L. Yu, L. Yang, Z. H. Huang, F. Kang and R. Lv, Journal of Energy Chemistry, 2021, **60**, 194–201.

S12 R. A. Marquez-Montes, K. Kawashima, Y. J. Son, J. A. Weeks, H. H. Sun, H. Celio, V. H. Ramos-Sánchez and C. B. Mullins, Journal of Materials Chemistry A, 2021, **9**, 7736–7749.

S13 G. Barati Darband, M. Aliofkhazraei, S. Hyun, A. Sabour Rouhaghdam and S. Shanmugam, Nanoscale, 2019, **11**, 16621–16634.

S14 C. S. Saraj, S. C. Singh, A. Shukla, W. Yu, M. U. Fayyaz and C. Guo, *ChemElectroChem*, 2021, **8**, 209–217.

S15 C. Jin, M. Hou, X. Li, D. Liu, D. Qu, Y. Dong, Z. Xie and C. Zhang, *Journal of Electroanalytical Chemistry*, 2022, **906**, 116014.

S16 M. M. Hasan, A. K. Gomaa, G. E. Khedr, K. E. Salem, B. S. Shaheen and N. K. Allam, *Energy & Fuels*, 2022, **36**, 14371–14381.

S17 J. Niu, Y. Yue, C. Yang, Y. Wang, J. Qin, X. Zhang and Z.-S. Wu, *Applied Surface Science*, 2021, **561**, 150030.